Formation of bimodal eutectic structure in $Ti_{63.5}Fe_{30.5}Sn_6$ and $Mg_{72}Cu_5Zn_{23}$ alloys

G.A. Song [a], J.H. Han [a], J.M. Park [b], S. Yi [c], D.H. Kim [b], K.B. Kim [a],*

[a] INAME & HMC, Faculty of Nanotechnology and Advanced Materials Engineering, Sejong University, 98 Gunja-dong, Gwangjin-gu, Seoul 143-747, Republic of Korea
[b] Center for Non-crystalline Materials, Department of Metallurgical Engineering, Yonsei University, 134 Shinchondong Seodaemungu, Seoul 120-749, Republic of Korea
[c] Department of Materials Science and Metallurgy, Kyungpook National University 1370 Sankyuk-dong, Buk-gu, Daegu 702-701, Republic of Korea

ARTICLE INFO

ABSTRACT

Microstructural investigation on $Ti_{63.5}Fe_{30.5}Sn_6$ and $Mg_{72}Cu_5Zn_{23}$ alloys reveals that bimodal eutectic structure containing the synchronization of structural and spatial heterogeneities in the spherical lamellar entity homogeneously forms upon solidification. Furthermore, the bimodal eutectic $Ti_{63.5}Fe_{30.5}Sn_6$ and $Mg_{72}Cu_5Zn_{23}$ alloys present the enhancement of both strength and plasticity at room temperature compared to the recently developed high strength Ti- and Mg-based alloys. This implies that the bimodal eutectic structure can be one of the effective ways to improve the plasticity of the high strength alloys.

© 2010 Elsevier B.V. All rights reserved.

1. Introduction

Nano/ultrafine grained materials or bulk metallic glasses have been highlighted due to an extraordinary high strength compared to conventional coarse grained materials [1–5]. However, these high alloys often exhibit limited macroscopic plastic strain at room temperature causing catastrophic failure. On the other hand, nanostructure-dendrite composites consisting of micro-scale dendrites homogeneously embedded in an ultrafine eutectic matrix have received extensive attention as a novel concept to enhance both strength and plasticity [6,7]. For example, a series of Ti-based nanostructure-dendrite composites comprising of micro-scale β-Ti solid-solution dendrites in nano-/ultrafine eutectic matrix processes a great combination of both ultimate compressive strength of ∼2.4 GPa and plasticity of ∼14% [6].

Recently, it has been reported that an outstanding mechanical properties under room temperature compression can be obtained by controlling the spatial heterogeneity, e.g. lamellar spacing, in Fe- [14] and Ti-based [15] alloys comprising fully eutectic structure without toughening phase, i.e. micro-scale primary dendrites. The detailed investigations on deformation behaviors of the ultrafine eutectic alloys reveals that a spatial heterogeneity, i.e. different lamellar spacing at the boundary of the eutectic colony, can be an origin to dissipate the localized stress by a rotation of the spherical eutectic colony. Along the line to improve the mechanical properties of such ultrafine eutectic alloys, there is an interesting finding

that micron-dendrite reinforced bimodal eutectic composites in Ti- [16] and Mg-based [17] alloys consisting of micro-scale dendrite phase in bimodal eutectic matrix introducing spatial, i.e. length scale and morphology, and structural heterogeneity, i.e. constitutive phases, exhibit excellent mechanical properties, i.e. strength and plasticity. Further detailed investigations on the deformation behavior of the micron-dendrite reinforced bimodal eutectic composites in Ti–Fe–Sn alloys reveal that typical slip-based deformation in the micro-scale Ti_3Sn primary dendrites possibly causes the enhancement of the macroscopic plastic deformation [18]. However, there is no trial to understand the role of the bimodal eutectic matrix on the deformation behavior.

In the present study, as a first step to interpret the effect of the bimodal eutectic structure on the strength and plasticity, we have successfully fabricated the bimodal eutectic structure in $Ti_{63.5}Fe_{30.5}Sn_6$ and $Mg_{72}Cu_5Zn_{23}$ alloys by systematically tuning the composition. By systematic investigations on the microstructure and mechanical properties of these alloys, it is possible to find out the important factors to enhance the plasticity of the bimodal eutectic alloys even without the micro-scale dendrites.

2. Experimental

A $Ti_{63.5}Fe_{30.5}Sn_6$ alloy was prepared by arc melting of the pure elements (purity > 99.8 wt%) under an argon atmosphere followed by direct casting into cylindrical rods with 3 mm diameter and 50 mm length using a suction casting facility. On the other hand, a $Mg_{72}Cu_5Zn_{23}$ alloy with a dimension of about 55 mm in length, 35 mm in width and 2–3 mm in thickness were prepared by induction melting with mixture of high purity elements (purity > 99.9 wt%) in the boron nitride (BN) coated graphite crucible under an argon gas atmosphere. Microstructure of these alloys was examined by scanning electron microscope (SEM, Jeol JSM-6390) and transmission electron microscope (TEM, Jeol-JEM 2010). Phase identification of the alloys was

* Corresponding author. Tel.: +82 2 3408 3690; fax: +82 2 3408 3664.
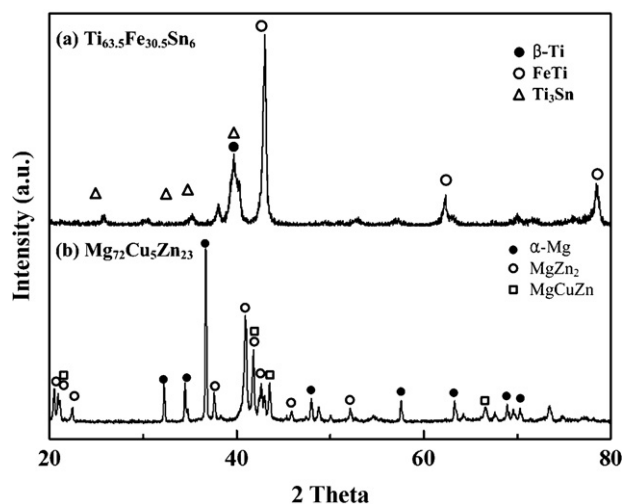E-mail address: kbkim@sejong.ac.kr (K.B. Kim).

Fig. 1. XRD traces of as-cast $Ti_{63.5}Fe_{30.5}Sn_6$ and $Mg_{72}Cu_5Zn_{23}$ alloys.

performed by X-ray diffraction (XRD, Rigaku-D/MAX-2500/PC) with Cu $K\alpha_1$ radiation ($\lambda = 1.5406$ Å). Thin foil samples for TEM analysis were prepared by conventional ion miller (Gatan Model-600). Cylindrical specimens with a 2:1 aspect ratio for compression tests of the $Ti_{63.5}Fe_{30.5}Sn_6$ alloy were prepared and bar shape specimens for compression tests of the $Mg_{72}Cu_5Zn_{23}$ alloy were prepared by machining the as-cast specimens to 2 mm × 2 mm cross section and 4 mm height. Mechanical properties were measured with an instron-type machine under uniaxial compression test at strain rate of 1×10^{-3} s^{-1} at room temperature more than 5 times to improve the reliability. In order to elucidate the macroscopic deformation mechanisms of these alloys, fracture surface of samples after compression tests were analyzed using SEM.

3. Results and discussion

Fig. 1(a) shows a XRD trace of as-cast $Ti_{63.5}Fe_{30.5}Sn_6$ alloys. The sharp diffraction peaks in Fig. 1(a) are identified as a mixture of a

bcc β-Ti (A2) solid solution, FeTi (B2) and hexagonal Ti_3Sn (D0$_{19}$) intermetallic compounds. Fig. 1(b) displays a XRD trace of as-cast $Mg_{72}Cu_5Zn_{23}$ alloy. The main sharp diffraction peaks in Fig. 1(a)–(d) is identified as a mixture of hexagonal α-Mg, hexagonal $MgZn_2$ and tetragonal MgCuZn phases.

Fig. 2 shows SEM backscattering electron (BSE) micrographs of as-cast $Ti_{63.5}Fe_{30.5}Sn_6$ [(a) and (b)] and $Mg_{72}Cu_5Zn_{23}$ [(c) and (d)] alloys. The BSE image of the as-cast $Ti_{63.5}Fe_{30.5}Sn_6$ alloy in Fig. 2(a) reveals that the bimodal eutectic structure consisting of a mixture of bright and gray contrast areas without the micro-scale primary dendrites forms homogeneously throughout the sample. The volume fraction of the bright and gray contrast areas is estimated to be 45.8% and 54.2%, respectively. Furthermore, one can find that the bright contrast area primarily forms on the matrix with the gray contrast. The BSE image of the as-cast $Ti_{63.5}Fe_{30.5}Sn_6$ alloy in Fig. 2(b) obtained at higher magnification clearly shows the detailed microstructure of the bimodal eutectic structure. One can find that the entity with the bright contrast is composed of typical laminated structure with an interlayer spacing of 200–300 nm whereas the entity with the gray contrast contains an irregular laminated structure with an interlayer spacing of 1–1.5 μm. Similarly, the BSE image of the as-cast $Mg_{72}Cu_5Zn_{23}$ alloys in Fig. 2(c) also reveals the formation of the bimodal eutectic structure. Moreover, the detailed microstructure shown in Fig. 2(d) exhibits that the bright contrast area consists of the typical laminated structure with an interlayer spacing of 300–400 nm. On the contrary, an interlayer spacing of the laminated structure in the dark contrast the matrix can be measured to be 1500–3000 nm. Based on the microstuctural investigation on the $Ti_{63.5}Fe_{30.5}Sn_6$ and $Mg_{72}Cu_5Zn_{23}$ alloys, it is considered that the bimodal eutectic structure with the structural and spatial heterogeneities successfully forms upon solidification.

Fig. 3 shows TEM bright-field images [(a), (b) and (g)] and selected area diffraction patterns [(c)–(f) and (h)–(j)] of the as-cast $Ti_{63.5}Fe_{30.5}Sn_6$ and $Mg_{72}Cu_5Zn_{23}$ alloys. Fig. 3(a) displays the
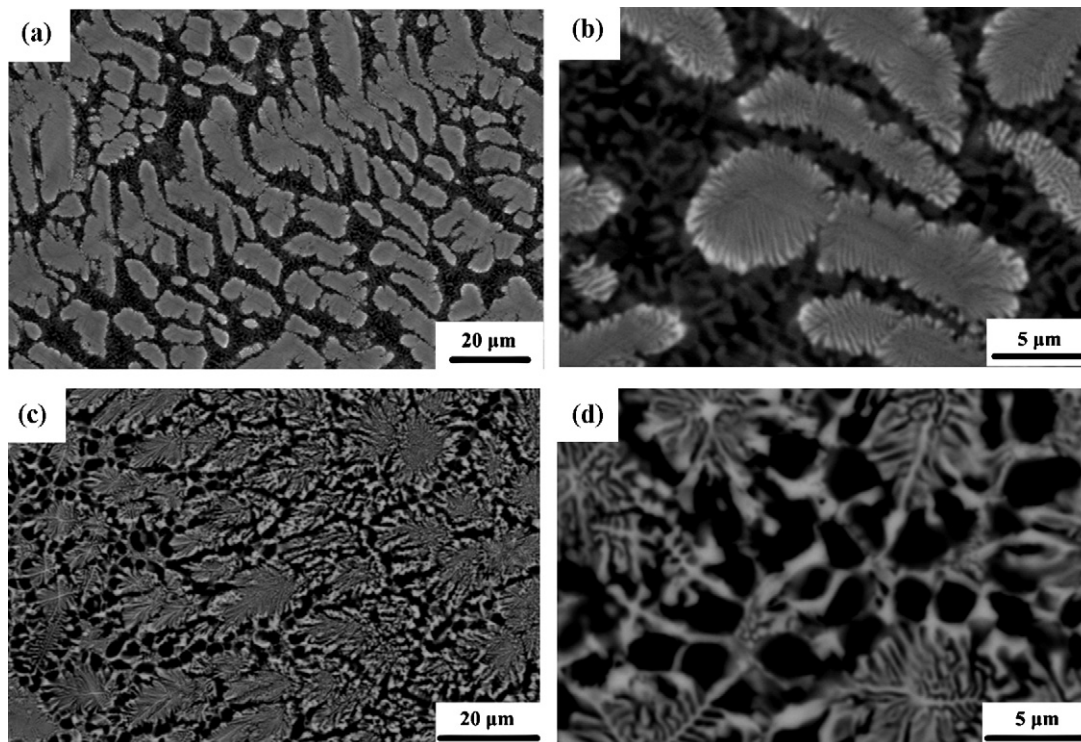

Fig. 2. SEM backscattering electron (BSE) micrographs of as-cast $Ti_{63.5}Fe_{30.5}Sn_6$ [(a) and (b)] and $Mg_{72}Cu_5Zn_{23}$ [(c) and (d)] alloys; [(a) and (c)]: overall microstructure and [(b) and (d)]: detailed microstructure at higher magnification.
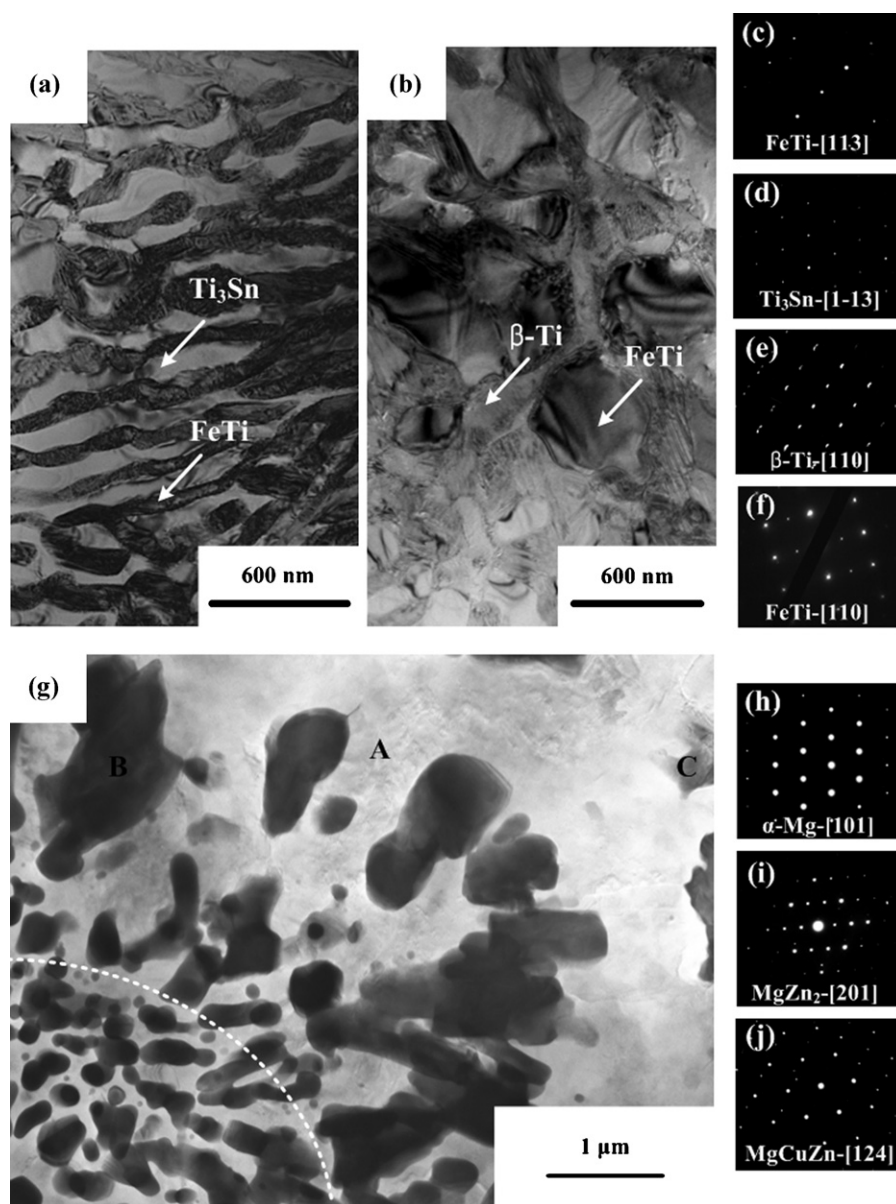
Fig. 3. TEM bright-field images and selected area diffraction patterns of the as-cast $Ti_{63.5}Fe_{30.5}Sn_6$ and $Mg_{72}Cu_5Zn_{23}$ alloys; (a) and (b): TEM images and (c)–(f): selected area diffraction patterns from the $Ti_{63.5}Fe_{30.5}Sn_6$ alloy, and (g): TEM image and (h)–(j): selected area diffraction patterns from $Mg_{72}Cu_5Zn_{23}$ alloy.

TEM bright field image obtained from the bright eutectic entity as shown in Fig. 2(a) and (b). The interlayer spacing is measured to be 150–250 nm. The EDX analysis of the bright and dark phases in the bright eutectic entity indicates that the bright and dark phases contain $Ti_{72.4}Fe_{3.08}Sn_{24.52}$ and $Ti_{53.85}Fe_{46.15}$, respectively. The SADPs in Fig. 3(c) and (d) obtained from the bright and dark phases in Fig. 3(a) correspond to the [1 1 3] and [1 −1 3] zone axes of the FeTi and Ti_3Sn phases, respectively. Fig. 3(b) displays the TEM bright field image obtained from the gray contrast entity as shown in Fig. 2(a) and (b). The interlayer spacing of the gray duplex area is estimated to be 900–1500 nm. The EDX analysis of the bright and dark phases indicates that the bright and dark phases consist of $Ti_{79.11}Fe_{10.89}Sn_{10.01}$ and $Ti_{54.69}Fe_{45.31}$, respectively. The SADPs in Fig. 3(e) and (f) obtained from the bright and dark phases of the gray contrast entity are identified as [1 1 0] and [1 1 0] zone axes of β-Ti and FeTi phases. Therefore, the TEM analysis strongly support the formation of the bimodal eutectic $Ti_{63.5}Fe_{30.5}Sn_6$ alloy consisting of a mixture of (FeTi + Ti_3Sn) and (β-Ti + FeTi) structures with both structural and spatial heterogeneities.

The TEM image in Fig. 3(g) obtained from the $Mg_{72}Cu_5Zn_{23}$ alloys displays that the length-scale of the fine and coarse eutectic structure is measured to be 300–400 and 1500–3000 nm, respectively, identical to the SEM analysis in Fig. 2(d). Moreover, the EDX analysis of the bright and dark phases in the fine eutectic entity indicates that the bright phase is very enriched in Mg content (94.35 at.%) whereas dark phase contains Mg (30.13 at.%), Zn (64.99 at.%) and Cu (4.88 at.%). Hence, it is possible to consider that the fine eutectic entity consists of a mixture of the α-Mg and $MgZn_2$ phases. On the contrary, the coarse eutectic entity can be distinguished into three areas from the contrasts, i.e. bright, gray and dark contrasts. The SADP in Fig. 3(h) obtained from the bright area marked by 'A' of the coarse eutectic area corresponds to the [1 0 1] zone axis of the α-Mg phase. The SADPs in Figs. 3(i) and (j) obtained from the areas B and C of the coarse eutectic area correspond to the [2 0 1] and [1 2 4] zone axes of the $MgZn_2$ and MgCuZn phases, respectively. Furthermore, the boundary between the fine and the coarse eutectic areas is quite continuous indicating the gradual modulation from the fine to coarse eutectic structure possibly due
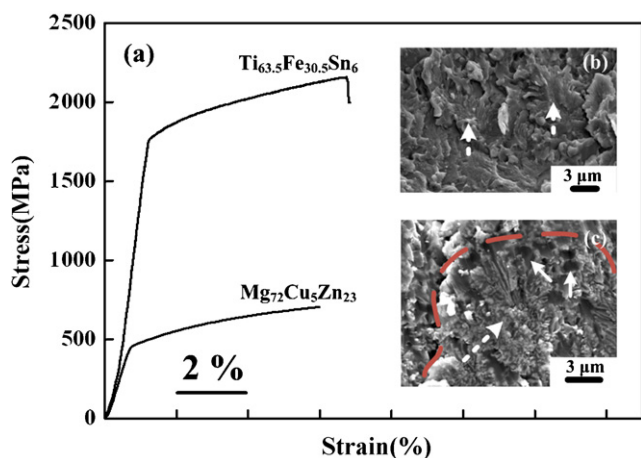
Fig. 4. Engineering stress–strain curves (a) of the $Ti_{63.5}Fe_{30.5}Sn_6$ and $Mg_{72}Cu_5Zn_{23}$ bimodal eutectic alloys at room temperature compression with inset SEM fractography (b) and (c), respectively.

to the solute partitioning. Therefore, it is clear that the fine eutectic area consists of the α-Mg and $MgZn_2$ phases whereas the coarse eutectic area contains the α-Mg, $MgZn_2$ and MgCuZn phases.

Fig. 4(a) shows engineering stress–strain curves of the $Ti_{63.5}Fe_{30.5}Sn_6$ and $Mg_{72}Cu_5Zn_{23}$ bimodal eutectic alloys at room temperature compression with inset SEM fractography. The $Ti_{63.5}Fe_{30.5}Sn_6$ bimodal eutectic alloy exhibits yield strength, σ_y, of 1799 MPa and plastic strain, ε_p, of 8.4%, respectively. One the other hand, the $Mg_{72}Cu_5Zn_{23}$ bimodal eutectic alloy shows yield strength, σ_y, of 455 MPa and plastic strain, ε_p, of 5%, respectively. Furthermore, the inset fractography in Fig. 4(b) from the $Ti_{63.5}Fe_{30.5}Sn_6$ hetero-duplex alloy displays that the cleavage is visible in the fine duplex area as marked by dot arrows. However, the several dimples characteristic of the ductile fracture of the sample can be found on the coarse eutectic entity. Fig. 4(c) shows the SEM images of the fracture surface of the $Mg_{72}Cu_5Zn_{23}$ bimodal eutectic alloy. As similar to Fig. 4(b), typical cleavage morphology on the fracture surface is visible in the fine eutectic structure as indicated by dot circles in Fig. 4(c). On the contrary, one can also find out that the several spherical dimples homogeneously form around the coarse eutectic structure as marked by arrows. Based on this finding, it is feasible to suggest that the strength of the $Ti_{63.5}Fe_{30.5}Sn_6$ bimodal eutectic alloy can be mainly contributed by the fine duplex entity. On the other hand, the coarse eutectic entity plays an important role to control the plasticity of the materials.

4. Summary

The $Ti_{63.5}Fe_{30.5}Sn_6$ bimodal eutectic alloy containing a mixture of the fine and coarse eutectic entities has been successfully developed in the present investigation. The detailed microstructural investigation indicates that the fine and coarse eutectic entities consist of a mixture of $(FeTi + Ti_3Sn)$ and $(\beta\text{-}Ti + TiFe)$ phases respectively. Furthermore, this bimodal eutectic alloy has high strength of 1799 MPa combined to large plastic strain of 8.4%. Similarly, the $Mg_{72}Cu_5Zn_{23}$ bimodal eutectic alloy with the spherical morphology of the boundary between the fine (i.e. α-Mg + $MgZn_2$ phases) and the coarse (i.e. α-Mg + $MgZn_2$ + MgCuZn phases) eutectic structures exhibits the high yield strength of $\sim$455 MPa as well as decent plasticity of $\sim$5%. Furthermore, the detailed investigation on the fracture surface indicates that the formation of the dimple fractography characteristic of the ductile deformation occurs at the coarse eutectic structure in both $Ti_{63.5}Fe_{30.5}Sn_6$ and $Mg_{72}Cu_5Zn_{23}$ bimodal eutectic alloys suggesting that the plasticity of the bimodal eutectic alloys can be originated from the coarse eutectic entity.

References

[1] H. Gleiter, Acta Mater. 48 (2000) 1–29.
[2] E. Ma, Met. Mater. Int. 10 (2004) 527.
[3] C.C. Koch, MRS Bull. 24 (1999) 54.
[4] A. Inoue, Nat. Mater. 2 (2003) 66.
[5] J.M. Park, Y.C. Kim, W.T. Kim, D.H. Kim, Mater. Trans. 44 (2004) 595–598.
[6] G. He, J. Eckert, W. Löser, L. Schultz, Nat. Mater. 2 (2003) 33.
[7] E. Ma, Nat. Mater. 2 (2003) 7–8.
[14] K.A. Song, J.S. Lee, J.S. Park, K.B. Kim, Met. Mater. Int. 15 (2009) 175–178.
[15] J. Das, F. Ettingshausen, J. Eckert, Scripta Mater. 58 (2008) 631–634.
[16] J.M. Park, S.W. Shon, T.E. Kim, D.H. Kim, K.B. Kim, W.T. Kim, Appl. Phys. Lett. 92 (2008) 091910.
[17] J. Das, K.B. Kim, F. Baier, W. Loser, J. Eckert, Appl. Phys. Lett. 87 (2005) 161907.
[18] J.M. Park, D.H. Kim, K.B. Kim, W.T. Kim, Appl. Phys. Lett. 91 (2007) 131907.

Further reading

[8] D.V. Louzguine, L.V. Louzguina, H. Kato, A. Inoue, Acta Mater. 53 (2005) 2009–2017.
[9] J.M. Park, S.W. Shon, T.E. Kim, D.H. Kim, K.B. Kim, W.T. Kim, Scripta Mater. 57 (2007) 1153–1156.
[10] K.B. Kim, J. Das, W. Xu, Z.F. Zhang, J. Eckert, Acta Mater. 54 (2006) 3701–3711.
[11] K.B. Kim, J. Das, F. Baier, J. Eckert, J. Alloy Compd. 434 (2007) 106–109.
[12] J.H. Han, K.B. Kim, S. Yi, J.M. Park, S.W. Sohn, T.E. Kim, D.H. Kim, J. Das, J. Eckert, Appl. Phys. Lett. 93 (2008) 141901.
[13] J.H. Han, K.B. Kim, S. Yi, J.M. Park, D.H. Kim, S. Pauly, J. Eckert, Appl. Phys. Lett. 93 (2008) 201906.
[19] K.B. Kim, J. Das, M.H. Lee, D.H. Kim, W.H. Lee, J. Eckert, Intermetallics 16 (2008) 538–543.
[20] J. Das, R. Theissmann, J. Eckert, Appl. Phys. Lett. 89 (2006) 261917.